Macromolecules
ARTICLE

Macromolecules **2009**, *42*, 6519–6528 **6519**
DOI: 10.1021/ma9007785

Structure−Activity Relationship in D-π-A-π-D-Based Photoinitiators for the Two-Photon-Induced Photopolymerization Process

Niklas Pucher,[†] Arnulf Rosspeintner,[‡] Valentin Satzinger,[§] Volker Schmidt,[§] Georg Gescheidt,[‡] Jürgen Stampfl,[⊥] and Robert Liska*,[†]

[†]*Vienna University of Technology, Institute of Applied Synthetic Chemistry, Division of Macromolecular Chemistry, Getreidemarkt 9/163/MC, 1060 Vienna, Austria,* [‡]*Graz University of Technology, Institute of Physical and Theoretical Chemistry, 8010 Graz, Austria,* [§]*Joanneum Research, Institute of Nanostructured Materials and Photonics, Franz Pichlerstr. 30, 8160 Weiz, Austria, and* [⊥]*Vienna University of Technology, Institute of Materials Science and Technology, Favoritenstrasse 9-11, 1040 Vienna, Austria*

Received April 9, 2009; Revised Manuscript Received July 17, 2009

ABSTRACT: This article presents the synthesis and characterization of a series of cross-conjugated D-π-A-π-D-based photoinitiators for the two-photon-induced photopolymerization process. Different donor and acceptor functionalities and derivatives containing double and triple bonds in the conjugated backbone allowed the evaluation of structure−activity relationship. Investigation of the basic photophysical properties showed high extinction coefficients at around 400 nm and none or vanishingly small emission quantum yields. The evaluated initiators showed at least similar activity, and in some cases broader processing windows than well-known highly active initiators from the literature and by far better results than commercially available initiators in terms of two-photon-induced microfabrication. These results are well in accordance with the TPA cross section values for the compounds measured by z-scan analysis. By using optimized parameters, structures with line widths of about 250 nm were obtained at photoinitiator concentrations as low as 0.05 wt %.

Introduction

In the past decade, two-photon-induced photopolymerization (TPIP)[1−6] has attracted much attention of researchers and has been intensely studied for various applications requiring three-dimensional (3D) structures with resolutions in the (sub)-micrometer range, such as different mechanical, electronic and optical microdevices,[1] high-density 3D optical data storage,[7] photonic crystals,[8] polymer-based optical waveguides on integrated circuit boards,[9−12] and the like. Furthermore, the high resolution and the versatility in the building process offer new routes for biomedical applications, such as tailored replacement materials.[13,14]

TPIP is a solid free-form fabrication technique where a resin, which contains mainly a multifunctional acrylate-based monomer and a photoinitiator (PI), is cured inside the focal point of a femtosecond pulsed near-infrared laser beam. With this unique process it is possible to produce complex 3D structures with resolutions (∼120 nm) below the diffraction limit of the utilized wavelength.[15] With advanced techniques such as the application of radical quenchers[16,17] or repolymerization techniques,[18] it is even possible to improve the feature resolution to 65 and 22 nm, respectively.

A highly active TPA PI plays a key role in order to obtain an efficient and clean polymerization and therefore high-quality structures. In the literature, the TPA cross section (1 GM = 10^{-50} m^4 s photon^{-1}) is the currently used value to characterize the activity of a TPA compound. It has to be noted that this value corresponds only on the absorption behavior of the compound similar to the extinction coefficient (ε) of one-photon absorption in Lambert−Beer's law, giving only a hint for the subsequent photoreactivity.[6]

*Corresponding author. E-mail: robert.liska@tuwien.ac.at.

At the initial stages of TPIP, research groups used typical commercially available radical PIs such as Irgacure 369.[1,8,19] Relatively high concentrations and laser intensities as well as long exposure times are required when structuring with these one-photon initiators.[5,20,21] The limited efficiency of these PIs can be ascribed to the rather low TPA cross section, normally less than 40 GM,[22] while higher radical formation quantum yields and initiation efficiency tend to compensate the low TPA cross-section values.[23] Under practical conditions, several research groups still prefer these initiators, but in the past few years there has been a growing need for special PIs optimized for the TPIP process with a high photoinitiating or sensitizing quantum yield under TPIP conditions.[6]

Up to now, a full understanding of the relationship of the molecular structure and the two-photon properties has still remained a big challenge. A high GM value combined with a high photoreactivity just like for normal one-photon initiators seems the goal to achieve. In recent literature, a large variety of TPA active compounds has been reported with—in some cases—enormous TPA cross sections.[24,25]

To obtain these high GM values, a planar π-system with a long conjugation length and with different functional donor (D) and/or acceptor (A) groups are important structural parameters.[24−26]

Two representative examples of high efficiency that are frequently reported in literature are *E,E*-1,4-bis[4′-(*N,N*-di-*n*-butylamino)styryl]-2,5-dimethoxybenzene (**R1**) and *E,E*-1,4-bis-[4′-(*N,N*-di-*n*-butylamino)styryl]benzene (**R2**), with TPA cross sections up to 995 GM at the maximum of the TPA absorption spectra (730 nm) (Figure 1).[26] These initiators are using an intramolecular charge transfer mechanism in the primary initiation step, followed by an intermolecular electron transfer.[27]

In addition to the planarity, the conjugation length of the chromophore, the type of D/A system and the type of the

Published on Web 08/06/2009

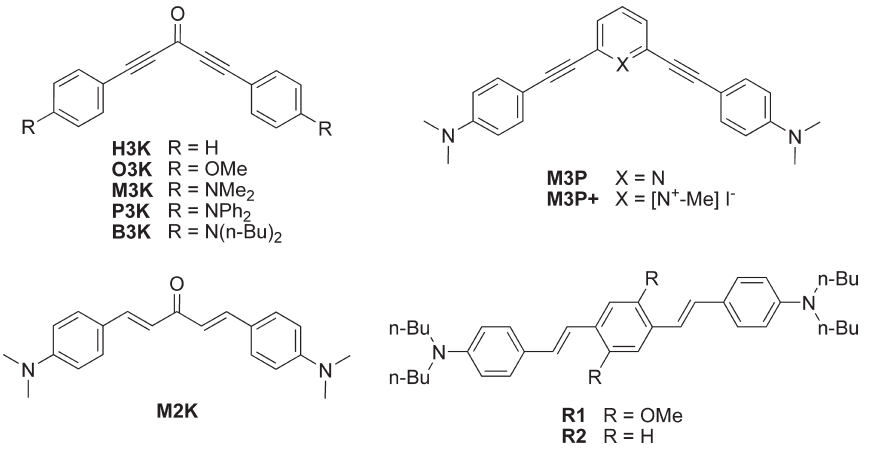

Figure 1. New TPA PIs and reference compounds.

conjugated π-backbone have a major influence on the photoactivity. Usually double bonds are used in the backbone of the PIs to extend the conjugation length due to their simple synthetic accessibility although the TPA cross section is normally lower than their triple-bond-containing counterparts.[28−32] However, double bonds tend to attenuate the desired photochemical processes by cis−trans isomerization.

Recently, we have shown that the triple-bond-containing 1,5-bis(4-(*N*,*N*-dimethylamino)phenyl)penta-1,4-diyn-3-one (**M3K**) serves as a highly sensitive and efficient TPA PI at low initiator concentrations in comparison to typical one-photon UV PIs,[20] although a rather low TPA cross section below 40 GM has been calculated for this compound very recently.[33] Investigations on the single-photon photochemistry of the unsubstituted **H3K** showed efficient hydrogen abstraction from H-donors like isopropyl alcohol.[34,35] In the presence of monomers [2 + 2] cycloaddition between the ketone of the initiator and the double bond of a nonpolymerizable monomer has been found in acetonitrile.[34]

Therefore, the aim of this paper was to investigate this triple-bond-containing, cross-conjugated and D-π-A-π-D-based lead structure. In order to study structure−activity relationship, variation of the functional donor (hydrogen, methoxy, dimethylamino, diphenylamino, and dibutylamino groups) and/or acceptor functionalities (ketone, pyridine, pyridinium) and moreover the influence of double and triple bonds located in the conjugated backbone were of interest (Figure 1).

Pyridinyl and pyridiniumyl moieties (**M3P**, **M3P**+) were chosen because of their strong electron acceptor properties. Structural relationship tests in the literature showed that these functionalities lead to high TPA cross sections compared to other acceptor groups although they are known as fluorescence dye compounds as well.[28,31,36] The 2- and 6-substituent positions of the pyridine were chosen because of the lower electron density and therefore higher acceptor ability compared to the positions 3 and 5. To determine the relevance of the triple bond in **M3K**, a derivative was synthesized with a double bond containing π-backbone (**M2K**). To test the different donor strength ($-$H < $-$OMe < $-NMe_2$ < $-NPh_2$) and its influence on the initiation activity several compounds (**H3K**, **O3K**, **M3K**, **P3K**) were synthesized and tested. Moreover, solubility in the resin is an important issue for the efficiency of TPA initiators.[6] This has been addressed by the introduction of butyl substituents in **B3K**.

For comparison, two highly potential TPA PIs, **R1** and **R2**, well-known from the literature,[26] and Irgacure 369 as a typical commercially available one-photon PI were tested.

For the characterization of the initiators, UV−vis absorption and emission measurements were carried out. As the determination of the TPA cross section gives only information on the absorption behavior[6] similar to ε of one-photon absorption in Lambert−Beer's law, we have decided to carry out TPIP structuring tests to characterize the new PIs. In the TPIP structuring tests, the ideal building parameters for each initiator were determined by changing the laser intensity, feed rate, and shape size using the same molar PI concentrations.

Experimental Section

Materials. All reagents were purchased from Sigma-Aldrich, Fluka, and ABCR and were used without further purification. The solvents were dried and purified by standard laboratory methods or were dried over Al_2O_3 cartridges. Trimethylolpropane triacrylate (**TTA**, Genomer 1330) and ethoxylated (20/3)-trimethylolpropane triacrylate (**ETA**, Sartomer 415) were received as a gift from Rahn and Sartomer, respectively. Petroleum ether (PE) refers to the fraction boiling in the range 40−60 °C. Column chromatography was performed with conventional techniques on VWR silica gel 60 (0.040−0.063 mm particle size). Aluminum-backed silica gel plates were used for TLC analyses.

Characterization. ^{1}H NMR (200 MHz) and ^{13}C NMR (50 MHz) spectra were measured with a BRUKER AC-E 200 FT-NMR-spectrometer. The chemical shift (s = singlet, bs = broad singlet, d = doublet, t = triplet, m = multiplet) is displayed in ppm using the nondeuterated solvent as internal standard. Solvents with a grade of deuteration of at least 99.5% were used. Melting points were measured on a Zeiss axioscope microscope with a Leitz heating block and remained uncorrected. The UV−vis absorption spectra were recorded either on a Hitachi U-2001 spectrometer or on a Shimadzu 3101-UVPC double-beam spectrometer, using slit widths of 2 nm. Spectroscopic grade solvents dried over molecular sieve and either 10 or 1 mm cuvettes were used for the measurements. Emission spectra were recorded on a thermostated Jobin Yvon FluoroMax-2 at 25 °C allowing for temperature control from 15 to 60 °C. The emission spectra were corrected according to the manufacturer specifications. Emission and excitation spectra were recorded on optically dilute solutions (OD < 0.1) in septa-sealed quartz cuvettes. The samples were deaerated by bubbling with argon during at least 10 min. The emission quantum yields were obtained using quinine sulfate in 0.5 M H_2SO_4 (10^{-5} M) as reference (φ_r = 0.55)[37] and the equation published by Kotelevskiy et al.[38]

GC-MS runs were performed on a Thermo Scientific DSQ II using a BGB 5 column (l = 30 m, d = 0.32 mm, 1.0 μm film; achiral). Elemental microanalysis was carried out with an EA 1108 CHNS-O analyzer from Carlo Erba at the microanalytical laboratory of the Institute for Physical Chemistry at the University of Vienna.

A Ti:sapphire laser system (100 fs pulse duration, 1 kHz repetition rate) was used for the open aperture z-scan analysis. A detailed description of the setup and the fitting equations used can be found elsewhere.[39] Rhodamine 6G and Rhodamine B in MeOH were used as reference standards in order to verify the reliability of the experimental setup.[40] All PIs were prepared as 1.0×10^{-2} M solutions in spectroscopic grade THF. The PI solutions were measured in a 0.2 mm thick flow cell in a nonrecycling volumetric flow of 5 mL/h. The excited volume is therefore refreshed approximately every 100 pulses, which approximately corresponds to 3 times for each *z*-position, which was found to be sufficient.

The measurements were carried out at different pulse energies in the range of 15−450 nJ. At even higher energies a signal of the pure solvent appears, and thermal effects are more likely to influence the measurement. Care had to be taken to collect the whole transmitted light in the far field using a big collecting lens. Additionally, a proper Gaussian beam profile in time and space is essential for the analysis.

Syntheses. (Dibromomethyl)triphenylphosphonium bromide,[41] 4-(ethynyl)-*N,N*-dimethylbenzeneamine (**2c**),[20] *N,N*-dimethyl-4-iodobenzeneamine (**4c**),[20] *N,N*-diphenyl-4-iodobenzeneamine (**4b**),[42] *N,N*-dibutyl-4-iodobenzeneamine (**4a**),[43] (1*E*,4*E*)-1,5-bis[4-(*N,N*-dimethylamino)phenyl]-1,4-pentadiene-3-one (**M2K**),[44] 1,5-bis(4-methoxyphenyl)penta-1,4-diyn-3-one (**O3K**),[20] *E,E*-1,4-bis[4′-(*N,N*-di-*n*-butylamino)styryl]-2,5-dimethoxybenzene (**R1**),[26] and *E,E*-1,4-bis[4′-(*N,N*-di-*n*-butylamino)styryl]benzene (**R2**)[26] were prepared according to the literature. Synthesis and characterization of the key intermediates 4-(4-(*N,N*-dibutylamino)phenyl)-2-methylbut-3-yn-2-ol (**1a**), 4-(4-(*N,N*-diphenylamino)phenyl)-2-methylbut-3-yn-2-ol (**1b**), 4-(ethynyl)-*N,N*-dibutylbenzeneamine (**2a**), and 4-(ethynyl)-*N,N*-diphenylbenzeneamine (**2b**) and NMR spectra of the new initiators are given in the Supporting Information. Spectral data were in agreement with the reported data. All reaction steps toward the final PI products were carried out in a special, light-protected room.

1,5-Bis[*4-*(*N,N-dibutylamino*)*phenyl*]*penta-1,4-diyn-3-ol* (***3a***). In a three-necked flask 1.21 g (5.25 mmol) of alkyne **2a** were dissolved in 50 mL of dry THF and 5.25 mmol of *n*-BuLi in hexane (2.01 mol/L) were added slowly at −50 °C under an argon atmosphere. After stirring for 45 min at this temperature, a quantitative deprotonation of the alkyne was detected by TLC and GC-MS studies (0.05 mL of the solution was quenched with 0.1 mL of freshly distilled trimethylsilyl chloride under inert atmosphere; afterward, a saturated $NaHCO_3$ solution was added dropwise to this mixture, which was then extracted with ethyl ethanoate (EE)). The mixture was cooled to −70 °C, and 0.19 g (2.56 mmol) of ethyl formate, dissolved in 5 mL of dry THF, was added dropwise via a syringe within 30 min. The solution was stirred for another 30 min at this temperature and was then allowed to warm up to −15 °C. The reaction was held at this temperature until TLC measurements showed a good yield for the alcohol **3a**. Afterward, the solution was hydrolyzed at −10 °C with a saturated $NaHCO_3$ solution (40 mL). The aqueous layer was extracted with chloroform (5 × 10 mL), and the combined organic layers were washed with a saturated NaCl solution and dried over Na_2SO_4. The solvent was removed in vacuum, and the residue was purified by column chromatography (PE:EE = 7:1) to give 0.71 g (56%) of **3a** as a yellow oil. ^{1}H NMR ($CDCl_3$): δ (ppm) = 7.31 (4H, d J = 9.00 Hz; ar−$H^{2,2',6,6'}$), 6.53 (4H, d J = 9.00 Hz; ar−$H^{3,3',5,5'}$), 5.56 (1H, d J = 7.24 Hz; −C*H*−OH), 3.26 (8H, t J = 7.73 Hz; 4 × −N−CH_2), 2.35 (1H, d J = 7.24 Hz; −CH−O*H*), 1.63−1.49 (8H, m, 4 × −N−CH_2−CH_2), 1.40−1.21 (8H, m; 4 × −CH_2−CH_3), 0.95 (12H, t J = 7.14 Hz; 4 × −CH_2−CH_3). ^{13}C NMR ($CDCl_3$): δ (ppm) = 148.34 (ar−$C^{4,4'}$), 133.30 (ar−$C^{2,6,2',6'}$), 111.17 (ar−$C^{3,3',5,5'}$), 107.66 (ar−*C*$^{1,1'}$), 85.72 (ar−*C*≡), 84.38 (−CH−*C*≡), 53.83 (−*C*H−OH), 50.79 (−N−*C*H_2), 29.47 (−N−CH_2−*C*H_2), 20.44 (−*C*H_2−CH_3), 14.11 (−CH_2−*C*H_3). Elemental Anal. Calcd for $C_{33}H_{46}N_2O$: C, 81.43; H, 9.53; N, 5.76. Found: C, 81.29; H, 9.62; N, 5.68.

1,5-Bis[*4-*(*N,N-diphenylamino*)*phenyl*]*penta-1,4-diyn-3-ol* (***3b***). **3b** was obtained by a coupling reaction of **2b** with ethyl formate according to the procedure described for **3a**. Purification by column chromatography (PE:EE = 7:1) gave **3b** (58%) as a yellow powder; mp 84−86 °C. ^{1}H NMR ($CDCl_3$): δ (ppm) = 7.34−7.24 (12H, m, ar−H), 7.12−7.03 (12H, m, ar−H), 6.97 (4H, d J = 8.74 Hz, ar−H), 5.56 (1H, d J = 7.4 Hz, −C*H*−OH), 2.11 (1H, d J = 7.1 Hz, −CH−O*H*). ^{13}C NMR ($CDCl_3$): δ (ppm) = 148.7 (ar−C^4), 147.4 (ar−$C^{1',1''}$), 133.2 (ar−$C^{2,6}$), 129.7 (ar−$C^{3',3'',5',5''}$), 125.4 (ar−$C^{3,5}$), 124.0 (ar−$C^{2',2'',6',6''}$), 122.24 (ar−$C^{4',4''}$), 114.9 (ar−C^1), 85.7 (ar−*C*≡C), 85.1 (ar−C≡*C*), 53.7 (−CH−OH). Elemental Anal. Calcd for $C_{41}H_{30}N_2O$: C, 86.90; H, 5.34; N, 4.94. Found: C, 87.10; H, 5.39; N, 4.92.

1,5-Bis(*4-*(*N,N-dibutylamino*)*phenyl*)*penta-1,4-diyn-3-one* (***B3K***). 0.831 g (9.55 mmol) of manganese(IV) oxide was added to a solution of 0.71 g (1.46 mmol) of **3a** in 100 mL of dry CH_2Cl_2. After stirring at ambient temperature for 52 h the reaction mixture was filtered using Hyflo, and the solvent was removed in vacuo. The solid residue was purified by column chromatography (PE:EE = 11:1) giving 0.58 g (83%) of **B3K** as slowly crystallizing substance; mp 68−70 °C. ^{1}H NMR ($CDCl_3$): δ (ppm) = 7.48 (H, d J = 9.00 Hz; −ar−$H^{2,2',6,6'}$), 6.57 (H, d J = 9.00 Hz; −ar−$H^{3,3',5,5'}$), 3.31 (H, t J = 7.92 Hz; 4 × −N−CH_2−), 1.66−1.56 (H, m; 4 × −N−CH_2−CH_2−), 1.45−1.25 (H, m; 4 × −CH_2−CH_3), 0.97 (H, t J = 7.14 Hz; 4 × −CH_2−CH_3). ^{13}C NMR ($CDCl_3$): δ (ppm) = 160.94 (C═O), 150.11 (ar−$C^{4,4'}$), 135.73 (ar−$C^{2,6,2',6'}$), 111.31 (ar−$C^{3,3',5,5'}$), 104.55 (ar−$C^{1,1'}$), 95.68 (ar−*C*≡), 91.44 (−CH−*C*≡), 50.87 (−N−*C*H_2−CH_2−), 29.44 (−N−CH_2−*C*H_2−), 20.42 (−*C*H_2−CH_3), 14.09 (−CH_2−*C*H_3). Elemental Anal. Calcd for $C_{33}H_{44}N_2O$: C, 81.77; H, 9.15; N, 5.78. Found: C, 81.72; H, 9.28; N, 5.61.

1,5-Bis(*4-*(*N,N-diphenylamino*)*phenyl*)*penta-1,4-diyn-3-one* (***P3K***). The PI **P3K** was obtained by oxidation reaction of **3b** with manganese(IV) oxide according to the procedure described for **3a**. The residue was purified by column chromatography (PE:EE = 7:1), giving the product in 97% yield as red solid; mp 190−193 °C. ^{1}H NMR ($CDCl_3$): δ (ppm) = 7.45 (4H, d J = 8.90 Hz, ≡−ar−$H^{2,6}$), 7.36−7.28 (8H, m, N−ar−$H^{2',2'',6',6''}$), 7.17−7.10 (20H, m, N−ar−$H^{3',3'',5',5''}$), 6.96 (4H, d J = 8.90 Hz, ≡−ar−$H^{3,5}$). ^{13}C NMR ($CDCl_3$): δ (ppm) = 160.82 (C═O), 150.66 (≡−ar−C^4), 146.44 (N−ar−$C^{1',1''}$), 135.00 (≡−ar−$C^{2,6}$), 129.78 (N−ar−$C^{3',3'',5',5''}$), 126.08 (N−ar−$C^{4',4''}$), 124.86 (N−ar−$C^{2',2'',6',6''}$), 120.38 (≡−ar−$C^{3,5}$), 110.78 (≡−ar−C^1), 93,52 (ar−C−*C*≡), 90.63 (CO−*C*≡). Elemental Anal. Calcd for $C_{41}H_{28}N_2O$: C, 87.21; H, 5.00; N, 4.96. Found: C, 87.15; H, 4.99; N, 4.81.

2,6-Bis[*2-*(*4-*(*N,N-dimethylamino*)*phenyl*)*ethynyl*]*pyridine* (***M3P***). 1.30 g of (5.49 mmol) 2,6-dibromopyridine and 2.00 g (13.77 mmol) of 4-(4-ethynyl)-*N,N*-dimethylbenzolamine (**2c**)[20] were dissolved in 250 mL of degassed and dry triethylamine under argon atmosphere. To this solution, 30 mg (0.16 mmol) of copper(I) iodide and 110 mg (0.16 mmol) of $PdCl_2$(btpp) were added, and the reaction mixture was stirred at room temperature overnight. The suspension was filtered and washed with 50 mL of Et_2O. The solvent was then removed under reduced pressure, and the brown residue was dissolved in chloroform and washed with brine. Afterward, the organic phase was dried over Na_2SO_4 and the solvent was evaporated. Finally, the product was purified by column chromatography (PE:EE = 3:1, neutral aluminum oxide) to obtain 1.04 g (52%) of **M3P** as a pale yellow solid; mp 262−264 °C. ^{1}H NMR ($CDCl_3$): δ (ppm) = 7.60 (1H, dd J = 8.02 Hz, py−H^4), 7.49 (4H, d J = 9.00 Hz, ar-$H^{2,2',6,6'}$), 7.36 (2H, d J = 7.62 Hz, py−$H^{3,5}$), 6.67 (4H, d J = 9.00 Hz, ar−$H^{3,3',5,5'}$), 3.00 (12H, s, 4 × −CH_3). ^{13}C NMR ($CDCl_3$): δ (ppm) = 150.82 (ar−$C^{4,4'}$), 144.73 (py−$C^{2,6}$), 136.42 (py−C^4), 133.72 (ar−$C^{2,2',6,6'}$), 125.31 (py−$C^{3,5}$), 112.01 (ar−$C^{3,3',5,5'}$), 109.09 (ar−$C^{1,1'}$), 91.63 (py−*C*≡−ar), 87.51 (py−≡*C*−ar), 40.51 (−CH_3). Elemental Anal. Calcd for $C_{25}H_{23}N_3$: C, 82.16; H, 6.34; N, 11.50. Found: C, 82.34; H, 6.52; N, 11.14.

Scheme 1. Syntheses of Terminal Alkyne Precursors

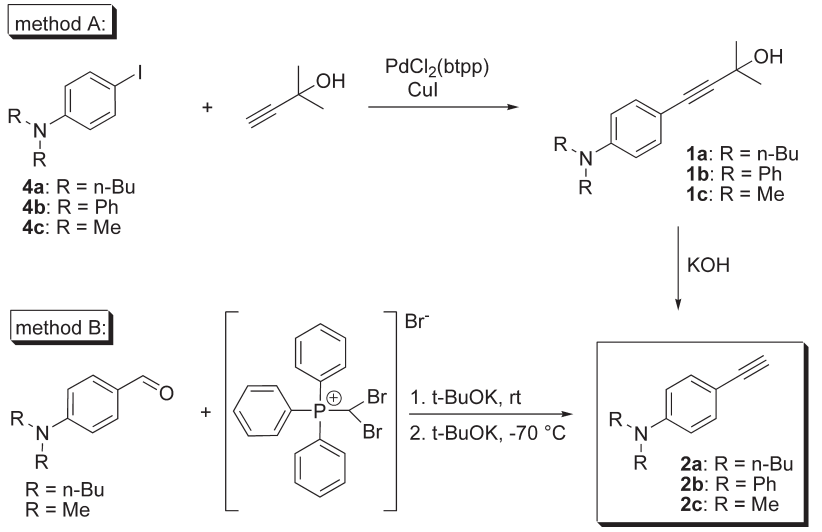

2,6-Bis[2-(4-(N,N-dimethylamino)phenyl)ethynyl]-1-methylpyridinium Iodide (***M3P***+). 350 mg (0.96 mmol) of pyridine **M3P** were dissolved in 140 mL of a 1:1 mixture of chloroform and THF under an argon atmosphere. 4.00 g (28.28 mmol) of methyl iodide was added slowly via a syringe, and the mixture was then stirred at room temperature for 7 days. The progress of the reaction was monitored by TLC ($CHCl_3$:MeOH = 7:1). The solvents and the excess of methyl iodide were carefully removed in vacuo, and the crude deep red precipitate was gently recrystallized from methanol to give a red solid in 59% yield; mp 215 °C (decomp). ^{1}H NMR (DMSO-d_6): δ (ppm) = 8.33 (1H, dd J = 8.01 Hz, py−H^4), 8.04 (2H, d J = 8.03 Hz, py−$H^{3,5}$), 7.62 (4H, d J = 8.83 Hz, ar−$H^{2,2',6,6'}$), 6.81 (4H, d J = 8.95 Hz, ar−$H^{3,3',5,5'}$), 4.41 (3H, s, py^+-CH_3), 3.04 (12H, s, 4 × −N−CH_3). ^{13}C NMR (DMSO-d_6): δ (ppm) = 152.05 (ar−$C^{4,4'}$), 142.48 (py−C^4), 138.63 (py−$C^{2,6}$), 134.32 (ar−$C^{2,2',6,6'}$), 128.14 (py−$C^{3,5}$), 111.89 (ar−$C^{3,3',5,5'}$), 109.89 (py−*C*≡−ar), 103.67 (ar−$C^{1,1'}$), 81.73 (py−≡*C*−ar), 44.48 (−N−*C*H_3), 39.61 (py−*C*H_3). Elemental Anal. Calcd for $C_{26}H_{26}IN_3$: C, 61.54; H, 5.16; N, 8.28. Found: C, 61.28; H, 5.47; N, 8.31.

TPIP Structuring Tests. *Laser Device*. Two different laser systems (system A and system B) were used for the direct laser writing of 3D structures. System A, which was used for the PI screening tests, is an amplified ultrafast Ti:sapphire laser system consisting of a Maitai-Spitfire combination from Spectra Physics.

The laser system operates at a repetition rate of 1 kHz and provides NIR pulses at 800 nm wavelength with a pulse duration of ∼130 fs. This amplified system achieves a maximum pulse energy of ∼1 mJ. An optical parametrical amplifier (OPA-800C) is used for structuring tests at 600 nm. The OPA extends the wavelength range of the laser system by means of harmonic generation and frequency mixing from 235 nm to 10 μm. The ultrafast OPA-800C is seeded by the amplified ultrafast laser pulses from the Spitfire, and the wavelength is—in this specific case—shifted by parametric conversion (second harmonic of the OPA signal) to 600 nm. Because of the conversion, the maximum pulse energy is less than 25 μJ, when pumped with 1 mJ pulses from the Spitfire. In case of 800 nm structuring the laser pulses are guided through an electro-optical switch that works also as laser attenuator by remote control of the crystal high voltage of the Pockels cell. Furthermore, a spatial filter improves fundamental spatial Gaussian beam distribution. The laser is focused into the sample by a 100× microscope objective (NA = 0.95). A He−Ne laser is collinearly guided to the sample, and the back-reflected light of the He−Ne laser is detected by a photodiode in a confocal setup, which permits the measurement of the sample's surface position and depth. The sample is moved by an Aerotech three axes stage relative to the laser focus in order to form a 3D structure (design of photonic structures by means of CAD modeling).

Additionally, to achieve higher resolutions of 3-dimensional structures, a different laser lithography system (Nanoscribe Photonic Standard, system B) was used. This system is equipped with a fiber laser, which provides NIR pulses at 780 nm wavelength with a pulse duration of ∼150 fs. The system operates at a repetition rate of 100 MHz. Direct laser writing with this system is usually carried out at a laser power below 7 mW (measured directly in front of the microscope objective). The laser is focused by a 100× oil immersion microscope objective (NA = 1.4), and the sample is mounted on a high-precision piezoelectric XYZ scanning stage with a 1 nm positioning accuracy.

General Procedure. For all samples the same fabrication process was implemented: The optical material was drop-cast onto a glass substrate. Subsequently, the samples were exposed to the laser beam, and the focus was scanned across the photosensitive material, which leads to an embedded 3D structure inside the material volume. After laser writing, the unexposed material was removed by development of the structure in methanol (rinsing). In a final step the samples were subjected to UV flood exposure to finally cure the optical material. The resulting structures, particularly their structural dimensions, integrity, and surface quality, were studied by means of SEM (JEOL JSM-5600).

Results and Discussion

Syntheses. Generally, the new amine-donor-containing derivatives **B3K** and **P3K** were prepared in a similar way to the synthesis of **M3K** (Scheme 2). The key intermediates were the terminal aryl acetylenes **2a** and **2b** (Scheme 1). There are several synthetic routes in the literature to obtain theses precursors. The most common is the reaction of a corresponding 4-iodobenzeneamine derivative under Sonogashira coupling conditions with either (trimethylsilyl)acetylene or 2-methyl-3-butyn-2-ol followed by a subsequent cleavage of the protection group in a second step (method A).[45,46] Furthermore, Michel et al.[47] published a Wittig-type one-pot synthesis starting from the corresponding aldehydes (method B). The advantages of the latter type of reaction compared to method A are the quick reaction time, the better commercial accessibility of the aldehydes, and the divergent

Scheme 2. Syntheses of M3K Derivatives

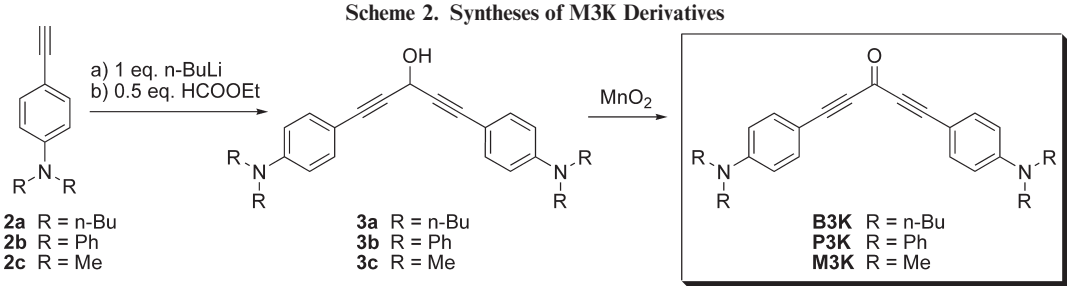

Scheme 3. Syntheses of PI M3P and M3P+

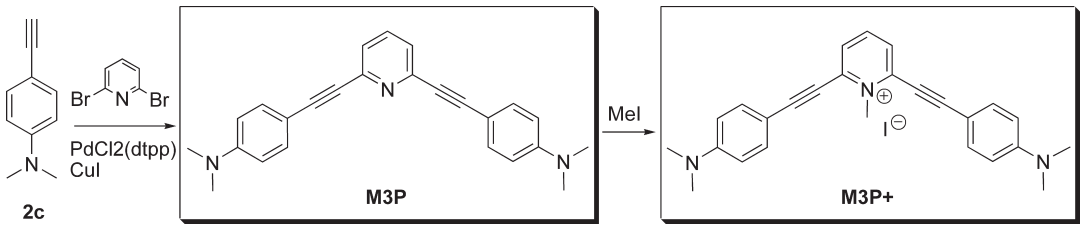

reaction pathway. The disadvantages are for sure the amount of Wittig salt and base needed resulting also in a more complicated purification step. Overall, both methods are suitable to obtain the precursors in high yields.

Method A was used first because it is the most common way in literature to synthesize terminal alkyne derivatives.[45] Therefore, the 4-iodobenzeneamine derivatives (**4a**−**c**) required for method A had to be synthesized according to different literature procedures. The methyl compound **4c** was recently prepared in our group by the reaction of *N,N*-dimethylbenzeneamine and I_2 in 64% yield.[20] The synthesis of *N,N*-diphenyl-4-iodobenzeneamine (**4b**) by a halogen exchange starting from *N,N*-diphenyl-4-bromobenzeneamine as proposed by Suh et al.[46] was not successful. Therefore, **4b** was synthesized according to Strohriegl et al.[42] using *N,N*-diphenylamine and 1,4-diiodobenzene as starting materials.

Synthesis of **4a** by para-iodation of *N,N*-dibutylbenzeneamine as for the preparation of **4c** is well-known from the literature but was not used to avoid the presence of iodine (impurities in the product). Therefore, the butyl derivative **4a** was obtained by alkylation of 4-iodobenzeneamine in high yields (78%).[43] This reaction was used to level out the possibility to introduce other functional groups in the final PI in further studies, which are not commercially available.

The reaction of these 4-iodobenzeneamine derivatives with 2-methyl-3-butyn-2-ol under Sonogashira conditions gave the protected alkyne products **1a**−**c** in yields between 70 and 88%. Finally, by deprotection under basic conditions the terminal alkynes **2a**−**c** were obtained in good yields (79−87%).

To evaluate the potential of method B, the terminal alkynes **2a** and **2c** were synthesized by a one-pot reaction of the corresponding aldehydes. By the use of a special Wittig-type salt and *t*-BuOK an intermediate was formed at room temperature and subsequently further addition of base at −70 °C yielded in the final products in 77% and 63%, respectively.

On the basis of the intermediates **2a** and **2b**, **B3K** and **P3K** were synthesized in a two-step reaction (Scheme 2). In the first step the terminal alkyne precursor was deprotonated with *n*-BuLi and then coupled with ethyl formate to obtain the corresponding alcohols **3a** (56%) and **3b** (58%). Subsequently, they were oxidized under mild conditions giving the PIs **B3K** and **P3K** in high yields (83−97%). It has to be mentioned that a scale up of this synthesis to 5 g of **B3K** was also successfully tested, and the solubility of **B3K** in various resins could be noticeably increased compared to other derivatives and the reference PIs.

The PIs **M3P** and **M3P**+ were obtained by a Sonogashira coupling reaction of the terminal alkyne **2c** with 2,6-dibromopyridine giving **M3P** in 52% yield. Subsequent treatment with methyl iodide gave the quaternized product **M3P**+ (59%) (Scheme 3).

Spectroscopy. Table 1 summarizes some of the basic one-photon photophysical properties for the PIs investigated, including the decadic molar extinction coefficient (ε_{max}), the absorption (λ_{abs}) and emission maxima (λ_{em}), the emission quantum yields (Φ_{em}) , and the TPA cross section (σ) values measured at 800 nm in THF.

In Figure 2, the one-photon absorption and emission spectra in acetonitrile and *n*-hexane are shown. In a previous publication[20] we have shown that the inclusion of donor groups, such as methoxy (**O3K**) or dimethylamino groups (**M3K**), into the *para*-position of the benzo-aromatic moiety led to bathochromic shifts in the absorption spectra by almost 0.3 and 1.0 eV, respectively. Additionally, ε_{max} showed a noticeable increase. From Figure 2 it is clear that substitution of the methyl groups at the amine by either butyl (**B3K**) or phenyl (**P3K**) alters the photophysical properties under investigation only marginally. The energy of the lowest energetic absorption transition is the same to within 0.08 eV for **M3K**, **B3K**, and **P3K**. Similarly, their Φ_{em}s are zero or vanishingly small.

Replacing the ketone-acceptor group by pyridine, **M3P**, leads to a substantial hypsochromic shift (almost 0.6 eV in acetonitrile) compared to **M3K**, while at the same time, Φ_{em} is significantly increased (from 0 to 0.58 in *n*-hexane). The formation of the pyridinium cation, **M3P**+, results in the total loss of emission and the appearance of a new absorption band shifted deeply into the visible region (λ_{abs} = 489 nm).

Substitution of the triple bond by a double bond gives **M2K**, which has already been used as an electron transfer sensitized PI in combination with iodonium salts.[49] Contrary to **M3K**, **M2K** shows at least in acetonitrile noticeable emission (Φ_{em} = 0.07), while the position of the absorption band remains basically unchanged.

Table 1. Collection of One- and Two-Photon Photophysical Properties of the Different PIs in Acetonitrile (First Value) and *n*-Hexane (Second Value) or in THF in the Case of TPA, Respectively[a]

PI	Φ_{em}		ν_{abs} [eV]		ν_{em} [eV]		λ_{abs} [nm]		λ_{em} [nm]		ε_{max}[b] [M^{-1} cm^{-1}]	σ[c] [GM]
H3K[d]	0.00	0.00	3.85	3.91			322	318			25 000	
O3K	0.02	0.00	3.50	3.63	2.25		352	342	526		32 000	< 10
M3K	0.00	0.00	2.84	3.14			434	394			53 000	165
B3K	0.00	0.00	2.76	3.07			449	404			65 000	238
P3K	8×10^{-4}	4×10^{-3}	2.82	3.00	1.80	2.84	438	412	650	433	50 000	256
M2K	0.07	0.00	2.84	3.09	2.11		434	400	569		48 000	261[e]
M3P	0.09	0.58	3.41	3.49	2.43	3.38	363	355	478	367	57 000	23
M3P+[f]	0.00		2.53				489				44 000	
R1	0.59	0.79	2.88	2.97	2.35	2.67	428	417	510	464	65 000	318
R2	0.65	0.88	3.00	3.10	2.40	2.83	410	400	504	437	57 000	314

[a] ν_{abs} and ν_{em} represent the energy of the absorption and emission maximum, respectively (using the transition moment representation).[48] [b] Measured in acetonitrile. [c] 1 GM = 10^{-50} m^4 s photon^{-1}. [d] The first vibronic transition was chosen (therefore the discrepancy with the value in Heller et al.).[20] [e] The broad signal may cause a certain error. [f] **M3P+** poor solubility in *n*-hexane, THF, and MeOH.

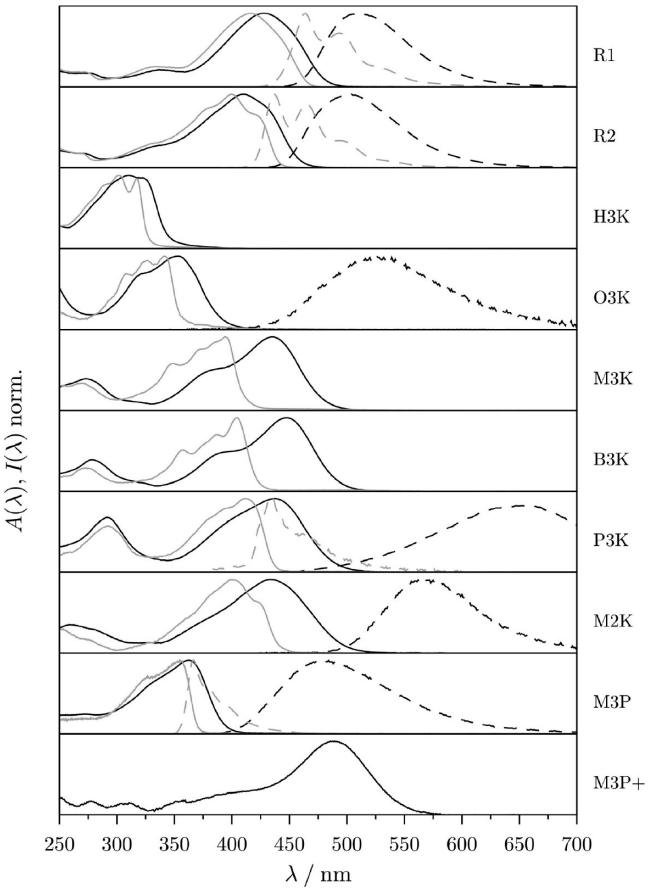

Figure 2. Absorption (full line) and emission (dashed line) spectra of **R1**, **R2**, **H3K**, **O3K**, and the novel PIs (**B3K**, **P3K**, **M2K**, **M3P**, **M3P+**) in *n*-hexane (gray) and acetonitrile (black).

The rather high ε_{max} ($> 1 \times 10^4$ M^{-1} cm^{-1}) as well as the bathochromic shifts in the absorption spectra when changing from polar acetonitrile to apolar *n*-hexane lead us to assign the transitions listed in Table 1 as $\pi-\pi^*$. Closer inspection of the absorption spectra reveals that **H3K** and **O3K** additionally possess an energetically lower lying and less intense band ($\varepsilon \sim 100$ M^{-1} cm^{-1}) at 3.1 eV ($\lambda = 400$ nm) with a negative solvatochromism which can be assigned to an $n-\pi^*$ transition. In the case of the amino-group-containing PIs (**M3K**, **B3K**, **P3K**) this band is not observable but masked by the bathochromically shifted strong $\pi-\pi^*$ transition.

For comparison, the photophysical properties of the well-known TPA PIs **R1** and **R2** were also evaluated. Absorption and emission maxima as well as emission quantum yields were found to be in good agreement with previous data.[24,27] While **R1** and **R2** exhibit strong fluorescence, the triple bond containing ketone-based PIs either do not show any or an extremely weak ($\Phi_{em} < 5 \times 10^{-3}$) emission, the nature of which (fluorescence or phosphorescence) is yet to be assigned.[50] These low emission quantum yields can be rationalized by an efficient intersystem crossing to the excited triplet state, as for example for the triple bond lacking PI analogue, benzophenone.[51] This is in line with our latest findings: that the step following photoexcitation is hydrogen abstraction of the triplet state from the solvent.[35]

To investigate the TPA properties of the evaluated PIs, an open aperture z-scan analysis[52] was performed to determine the TPA cross section at the wavelength of 800 nm. A nonrecycling flow cell geometry was used for the measurements because of a strong photodegradation of some PIs during the tests (especially the ketone-based PIs). This phenomenon was also described by Schafer et al.[22] and was furthermore described as an indicator for an effective two-photon initiator. In the Supporting Information the photodegradation of **P3K** is shown as a representative example at different volumetric flow rates. This test was carried out for each compound. The results indicated that a flow rate of 5 mL/h is sufficient for all PIs to wash away the irradiated sample out of the focal volume in a reasonable time.

The experimental data were fitted using the adopted equations of Sheik-Bahae et al.[52] in order to obtain the TPA cross section (σ) (Figure 3a). To exclude excited-state absorption and to proof the fact that a pure σ is determined, the measurements were repeated at different peak intensities and the calculated parameter q_0 scales linearly with intensity (Figure 3b).[52] All calculated σ values are given in Table 1.

The values for the TPA cross sections of the ketone-based initiators show an increase with enhanced donor strength of the substituents in the para position of the aromatic ring. No signal could be detected for **H3K**, and only a very low signal was measured in case of **O3K** at the given wavelength. Among the amino-based derivatives **P3K** had the highest value of 256 GM. Surprisingly, there is a significant difference between the methyl and butyl derivative **M3K** and **B3K**, maybe due to a shift of the TPA spectra between these two initiators, similar to the differences also observed in the one-photon spectra (Table 1).

The value for **M2K** is on the same order of magnitude as the other amino-ketone-based PI. A comparison with literature data[53] revealed that similar double-bond-containing derivatives are in the same range and also showing broader signals than the triple bond analogues that allows less accurate fitting of the data.

The low value for **M3P** might be explained by the weak acceptor capability of the pyridine moiety. Higher acceptor strength can be expected in the case of **M3P+**. Because of the

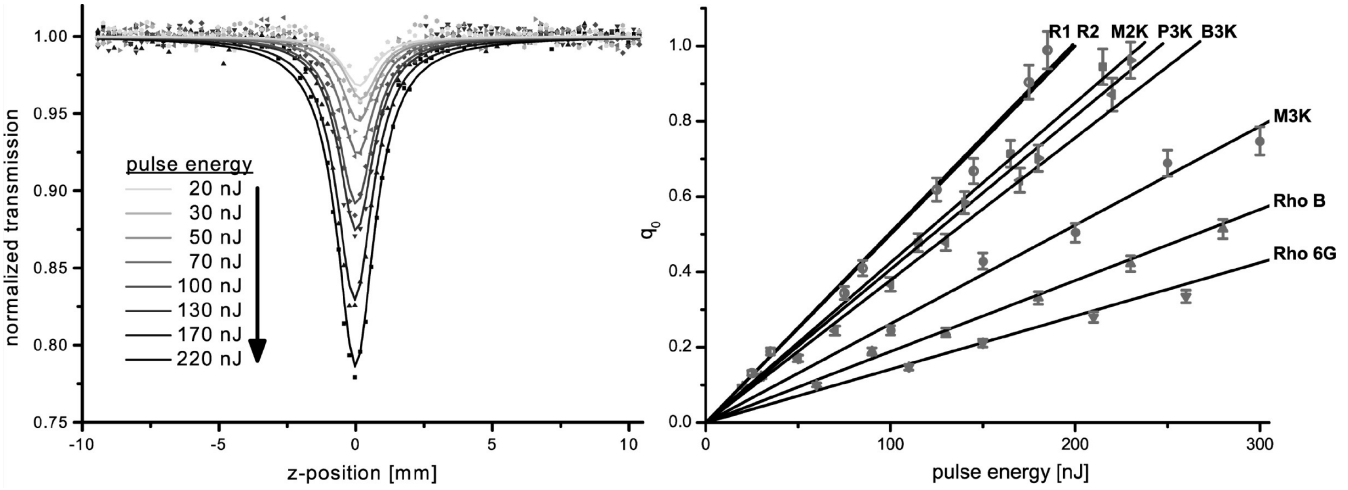

Figure 3. (a) Experimental z-scan data (dots) and fitting curves (full lines) for **B3K** at different pulse energies. (b) q_0 plotted vs intensity for investigated PIs and an example for standard measurement and fitting data.

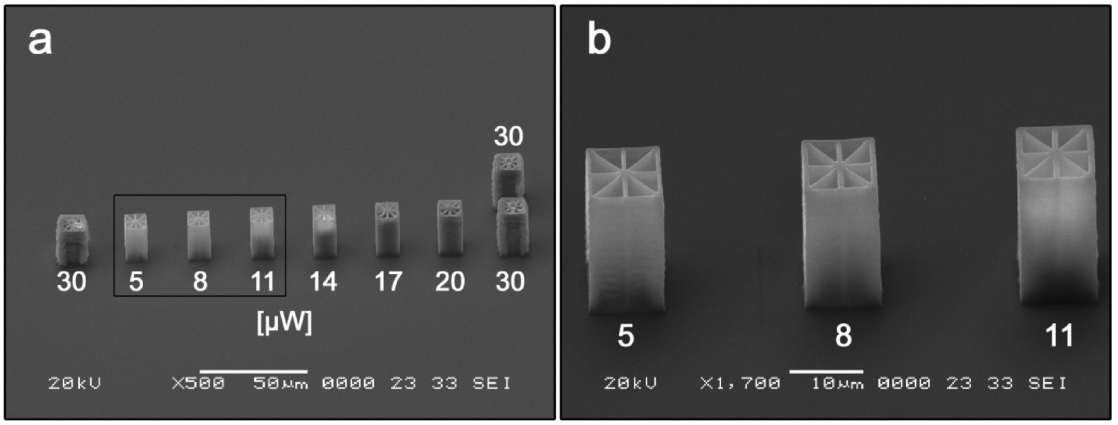

Figure 4. (a) Screening of PI **B3K** (range 5−30 μW). (b) Detailed view.

poor solubility, only very low concentrations with poor signal-noise ratio could be measured. From these data we can only assume that the **M3P**+ has a significantly higher value than **M3P**.

The references **R1** and **R2** showed slightly higher values than the ketone-based initiators. Compared to data from literature at 800 nm,[26,54] results are quite satisfactory keeping in mind that a comparison with literature values is quite complicated because of the different experimental methods (two-photon fluorescence), pulse durations, and solvents used for measuring.[40]

Therefore, relative comparisons are more useful as it is also true for TPIP structuring.

TPIP Structuring Tests. In order to estimate the activity of the PIs, defined test structures (lateral dimension: 10 × 10 and 25 μm in height) were written into the material by means of TPIP. The laser intensity was screened in a range of 1−100 μW with laser system A (Figure 4). A 1:1 mixture of ETA/TTA was used as an acrylate-based test resin as good results had been achieved in previous studies.[20] For all studies the same molar PI concentration of 6.3×10^{-6} mol PI/g resin (which corresponds to 0.2 wt % of **M3K**) was employed in order to have the option to compare directly the TPIP activities of the PIs. To determine the threshold of the photoinitiating ability, the tests were repeated with lower molar PI concentrations (1.6×10^{-6} and 1.6×10^{-7} mol PI/g resin, which corresponds to 0.05 and 0.005 wt % of **M3K**, respectively). A first broad screening test at different laser intensities revealed the possible processing window, which was studied in detail in a second test.

The different shades of gray of the bars and their corresponding numbers in Figure 5 indicate the quality of the structures. At the lower end of each ideal processing window in the diagram, no well-connected structures could be obtained after the standard post processing procedure as the threshold of initiation is reached. Above that, the numbers 1 and 2 define nicely structured shapes with a high resolution and a smooth surface quality (Figure 6). Generally, broader "perfect" processing windows (1, 2) and lower laser intensities are desired in terms of high throughput in mass production because this enables a splitting of the initial laser beam for parallel processing with multiple laser heads at high feed rates. Additionally, decomposition of the material by thermal effects can be avoided. With structure quality 3, the shapes tend to lose their resolution and their smooth surfaces. So these laser intensities are still useful for larger parts but not perfect for high-resolution TPIP. Parts structured with laser intensities giving quality 4 no longer showed acceptable results. The walls had several imperfections such as holes or no well-defined structures due to overexposure. In the case of quality 5 the shapes are no longer identifiable because of several defects such as complete missing walls and vast holes (Figure 6y) or due to massive over exposure effects, which could be recognized by "exploded shapes" (Figure 6x).

In our measurements, the initiators (6.3×10^{-6} mol PI/g resin) well-known from the literature (**R1**, **R2**) are both able to build up nicely shaped structures at low laser intensities. The commercially available PI Irgacure 369 showed no good results at 800 nm at the given low PI concentration, which is well in agreement with the low TPA cross section.[22] Because of the TPA spectrum of Irgacure 369 ($\lambda_{max} = 324$ nm),[22] the laser wavelength was adjusted to 600 nm. At this wavelength, only a small processing window of less than 10 μW was found, where sufficiently good results can be obtained. It has to be mentioned that by increasing the concentration of Irgacure 369 to 1 wt %, which is a common concentration found in the literature, nicely exposured structures between 4 and 7 μW could be obtained at 600 nm. The same effect could also be observed when using the presented initiators.

The starting point for our investigations was **M3K** that gave good results in preliminary tests. By changing the acceptor group in **M3K** from a carbonyl group to a pyridine moiety as in PI **M3P**, the solubility was dramatically decreased. In the structuring tests we were not able to obtain any good results with the pyridine-based compound **M3P** (data not shown). Explanation might be given by the low TPA cross section and the inability for hydrogen abstraction reactions compared to ketone-based PIs. Nevertheless, in the case of a pyridinium ion as a functional acceptor group as in **M3P+**, the solubility in the resin as well as the activity and the ideal processing window could be improved compared to **M3P**, although it is still lower than that of the carbonyl-containing **M3K**.

Despite the higher TPA cross section, the easily accessible double-bond derivative **M2K** gave significantly lower initiation ability compared to the triple-bond-containing **M3K**.

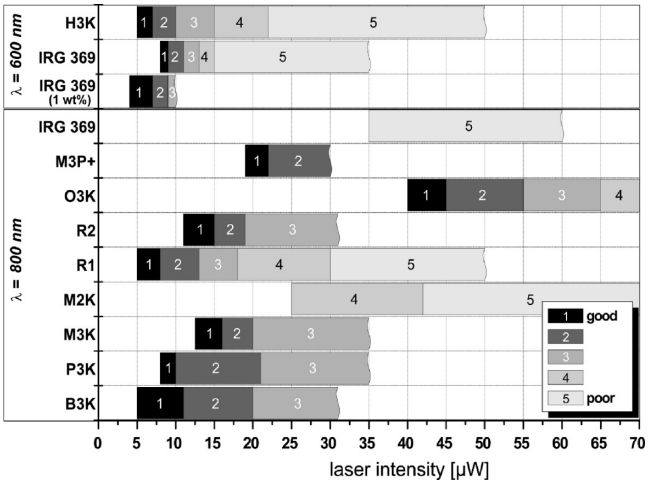

Figure 5. PI TPIP screening tests (PI concentration: 6.3×10^{-6} mol PI/g resin).

The reason could be an unwanted photochemical cis−trans isomerization reaction as mentioned above.

In accordance with the z-scan measurements, the total absence of a good donor group in case of **H3K** gave no good results at 800 nm. By adopting the laser wavelength to 600 nm as with Irgacure 369, nicely shaped structures could be produced in a small area at low intensities. Combined with the tuned laser wavelength, the higher photochemical reactivity of **H3K** and Irgacure 369 compared to true TPA PIs is very likely the reason for still giving nice results in a narrow structuring area. The use of the methoxy functionality as a weaker donor group in case of **O3K** not only resulted in a very poor TPA cross section but also by far higher laser intensities were required. As a side note, the thiomethyl derivative (**S3K**), having a stronger electron-donating group, tested in a previous study was not able to give good results at any laser intensity.[20]

The different derivatives based on the amino-based donor (**M3K**, **P3K**, and **B3K**) showed very good results in these tests. The ideal processing window is broader than that of the references, and the laser intensities required are quite low. When comparing the three different donor groups in agreement with the z-scan values, the additional phenyl groups of **P3K** had a positive effect on the activity compared to **M3K**, but in this case the solubility in the resin was significantly lowered. The butyl side chains of **B3K** have the best influence on the activity. As described in the literature,[3] the increased solubility seems to be the reason for that. So **B3K** turned out to be the best performing initiator in our tests having the broadest ideal structuring process window at laser intensities as low as 5 μW and a very good solubility in the resin.

The tests were repeated also with lower molar PI concentrations in order to determine the lowest possible PI concentration under these conditions (data not shown). For the medium concentration (1.6×10^{-6} mol PI/g resin) the results for all initiators are very similar to the higher concentration; only the ideal processing window is slightly shifted to higher laser intensities. At the lowest concentration (1.6×10^{-7} mol PI/g resin), only **H3K** could produce well-defined structures within a very small process window at 600 nm.

Additionally, more complex 3D structures were inscribed into the material volume using **B3K** (6.3×10^{-6} mol PI/g resin) as initiator. A laser power of 11 μW at a given feedrate of 1 mm/min allowed the structuring of a dragonfly and a dinosaur sculpture using laser system A (Figure 7a,b). These shapes are showing perfectly the advantages of TPIP compared to other rapid prototyping techniques. High resolutions, which are otherwise inaccessible, and complex 3D structures with massive overhangs such as the wings of the dragonfly sculpture (Figure 7a) can be obtained easily.

Furthermore, a different laser system with a repetition rate of 100 MHz (system B) was also tested in order to achieve higher resolutions than obtained by system A. In a power range of 1.5−2.8 mW at a feed rate of 10−25 μm/s perfectly

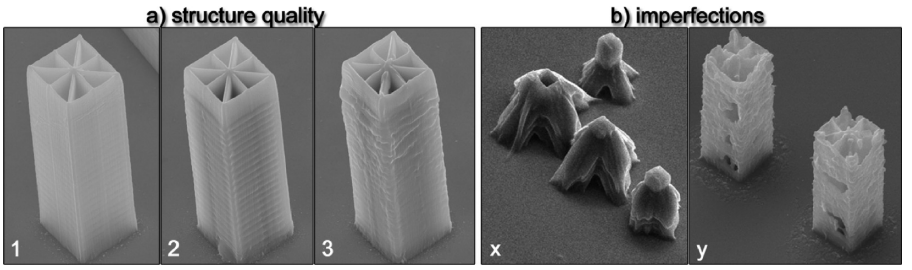

Figure 6. (a) Typical qualities of the shapes from very good (1) to average (3) (4 and 5 are not shown). (b) Typical imperfections of the structures at higher laser intensities such as over exposure (x) and holes (y).

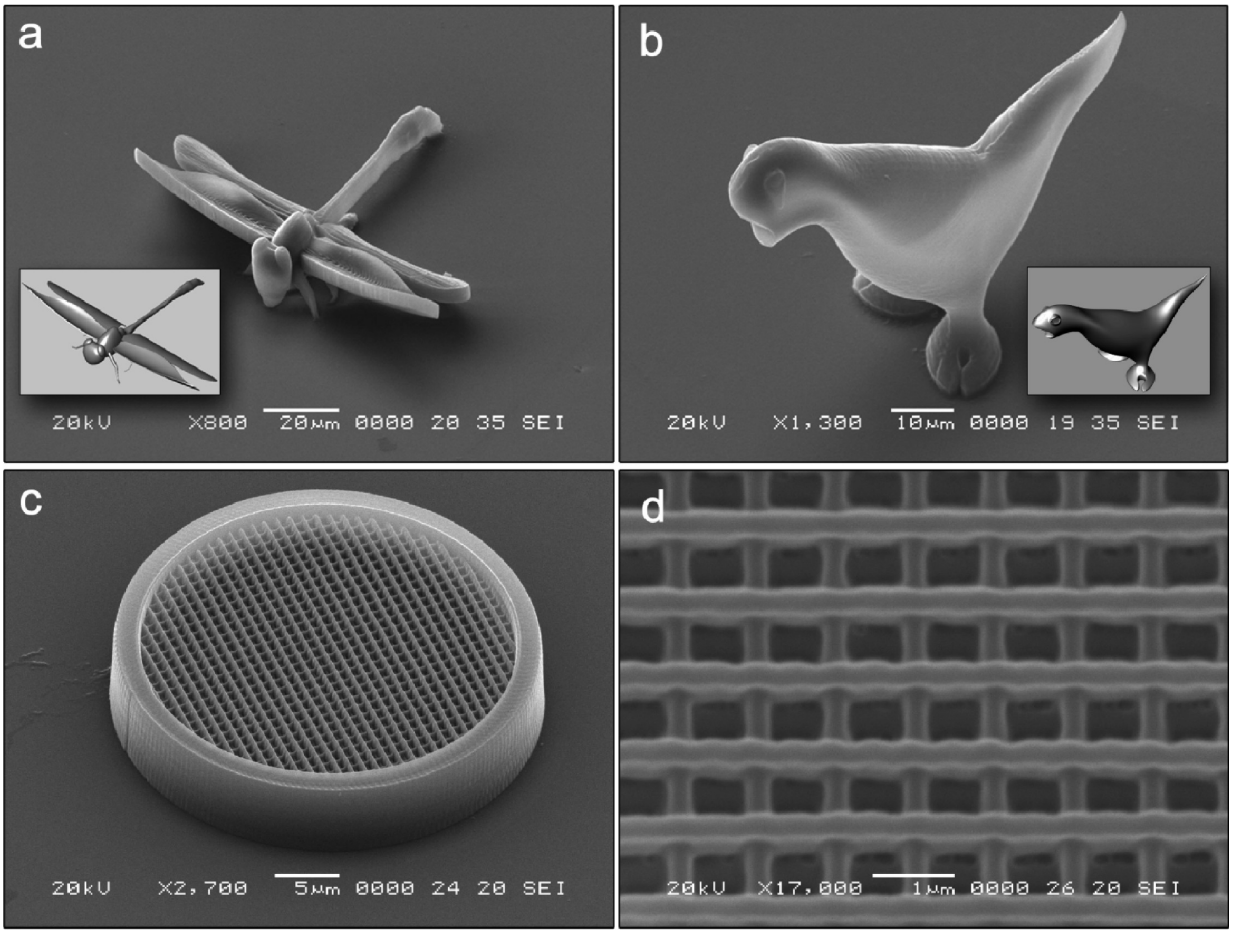

Figure 7. 3D structures (resin ETA/TTA 1:1, **B3K** as initiator) using different laser systems: system A (1 kHz): (a) dragonfly;[55] (b) dinosaur;[55] system B (100 MHz): (c) woodpile structure; (d) detailed view of the woodpile structure.

developed woodpile structures with and without supporting wall were prepared (Figure 7c,d). Line widths of about 250 nm were obtained and could be further improved by an optimal laser system setup such as optimized laser power-feed rate ratio, a shaded ring filter, and the like.

Conclusion

In summary, we report on the successful syntheses and evaluation of a series of radical PIs optimized for the usage in TPIP processes containing different donor and acceptor functionalities as well as double and triple bonds in the conjugated-π-backbone. On the basis of the recently published triple-bond-containing Michler's ketone derivative **M3K**, several other PIs were synthesized in order to study the structure−activity relationship. Generally, structuring tests are well in accordance with the values for the TPA cross section; only in the case of double-bond-containing derivatives such as **M2K** significantly lower activity has to be accepted presumably due to cis−trans isomerization reactions. A carbonyl group as electron withdrawing functionality showed by far better results than pyridinyl and pyridiniumyl moieties. A dibutylamino functionality increased the activity of the PIs under TPIP conditions compared to dimethylamino and diphenylamino electron-donating groups most likely due to an improved solubility in the resin. Therefore, **B3K** turned out to contain the optimum set of functional groups at the given lead structure, having the highest activity of all presented initiators.

To conclude, the new compounds are highly efficient initiators similar to other very potential two-photon initiators from the literature. We were able to produce nicely shaped structures with PI concentrations as low as ~0.05 wt %. Additionally, the ideal processing window for each initiator was determined by changing the laser intensity and initiator concentration at a fixed feed rate. By using optimized parameters, structures with line widths of about 250 nm were obtained.

As there are presumably different mechanisms of initiation responsible, a more comprehensive study on the photophysics and theoretical and experimental cross-section values of the new PIs is currently in progress and will be the subject of a separate publication.

Acknowledgment. We thank Ali A. Ajami and Wolfgang Husinsky (IAP, TU Vienna) for the help in measuring the TPA cross section with z-scan analysis. We acknowledge the financial support by the Austrian Science Fund (FWF) and the Austrian Research Agency (FFG) under Contracts N703 (STRUCMAT-ISOTEC) and P18623 N-17.

Supporting Information Available: Synthesis and characterization of the key intermediates, NMR spectra of the new initiators, and photodegradation effect at different flow rates (z-scan analysis). This material is available free of charge via the Internet at http://pubs.acs.org.

References and Notes

(1) Maruo, S.; Nakamura, O.; Kawata, S. *Opt. Lett.* **1997**, *22* (2), 132–134.
(2) Maruo, S.; Fourkas, J. T. *Laser Photonics Rev.* **2008**, *2* (1−2), 100–111.
(3) Sun, H.-B.; Kawata, S. *Adv. Polym. Sci.* **2004**, *170*, 169−273.

(4) Sun, H.-B.; Kawata, S. *J. Lightwave Technol.* **2003**, *21* (3), 624–633.
(5) Wu, S.; Serbin, J.; Gu, M. *J. Photochem. Photobiol., A* **2006**, *181* (1), 1–11.
(6) Lee, K.-S.; Kim, R. H.; Yang, D.-Y.; Park, S. H. *Prog. Polym. Sci.* **2008**, *33* (6), 631–681.
(7) Parthenopoulos, D. A.; Rentzepis, P. M. *Science* (*Washington, D. C.*) **1989**, *245* (4920), 843–5.
(8) Sun, H.-B.; Matsuo, S.; Misawa, H. *Appl. Phys. Lett.* **1999**, *74* (6), 786–788.
(9) Infuehr, R.; Pucher, N.; Heller, C.; Lichtenegger, H.; Liska, R.; Schmidt, V.; Kuna, L.; Haase, A.; Stampfl, J. *Appl. Surf. Sci.* **2007**, *254* (4), 836–840.
(10) Satzinger, V.; Schmidt, V.; Kuna, L.; Palfinger, C.; Infuehr, R.; Liska, R.; Krenn, J. R. *Proc. SPIE* **2008**, *6992*, 699217/1−699217/10.
(11) Schmidt, V.; Kuna, L.; Satzinger, V.; Jakopic, G. *J. Laser Micro/Nanoeng.* **2007**, *2* (3), 170–177.
(12) Krivec, S.; Matsko, N.; Satzinger, V.; Pucher, N.; Galler, N.; Koch, T.; Schmidt, V.; Grogger, W.; Liska, R.; Lichtenegger, H., manuscript in preparation.
(13) Ovsianikov, A.; Schlie, S.; Ngezahayo, A.; Haverich, A.; Chichkov Boris, N. *J. Tissue Eng. Regener. Med* **2007**, *1* (6), 443–9.
(14) Claeyssens, F.; Hasan, E. A.; Gaidukeviciute, A.; Achilleos, D. S.; Ranella, A.; Reinhardt, C.; Ovsianikov, A.; Shizhou, X.; Fotakis, C.; Vamvakaki, M.; Chichkov, B. N.; Farsari, M. *Langmuir* **2009**, *25* (5), 3219–3223.
(15) Tanaka, T.; Sun, H.-B.; Kawata, S. *Appl. Phys. Lett.* **2002**, *80* (2), 312–314.
(16) Takada, K.; Sun, H.-B.; Kawata, S. *Appl. Phys. Lett.* **2005**, *86* (7), 071122/1–071122/3.
(17) Park, S. H.; Lim, T. W.; Yang, D.-Y.; Kim, R. H.; Lee, K.-S. *Macromol. Res.* **2006**, *14* (5), 559–564.
(18) Park, S. H.; Lim, T. W.; Yang, D.-Y.; Cho, N. C.; Lee, K.-S. *Appl. Phys. Lett.* **2006**, *89* (17), 173133/1–173133/3.
(19) Nguyen, L. H.; Straub, M.; Gu, M. *Adv. Funct. Mater.* **2005**, *15* (2), 209–216.
(20) Heller, C.; Pucher, N.; Seidl, B.; Kalinyaprak-Icten, K.; Ullrich, G.; Kuna, L.; Satzinger, V.; Schmidt, V.; Lichtenegger, H. C.; Stampfl, J.; Liska, R. *J. Polym. Sci., Part A: Polym. Chem.* **2007**, *45* (15), 3280–3291.
(21) Baldacchini, T.; LaFratta, C. N.; Farrer, R. A.; Teich, M. C.; Saleh, B. E. A.; Naughton, M. J.; Fourkas, J. T. *J. Appl. Phys.* **2004**, *95* (11), 6072−6076.
(22) Schafer, K. J.; Hales, J. M.; Balu, M.; Belfield, K. D.; Van Stryland, E. W.; Hagan, D. J. *J. Photochem. Photobiol., A* **2004**, *162* (2−3), 497–502.
(23) Li, L.; Fourkas, J. T. *Mater. Today* (*Oxford, U.K.*) **2007**, *10* (6), 30–37.
(24) Albota, M.; Beljonne, D.; Bredas, J.-L.; Ehrlich, J. E.; Fu, J.-Y.; Heikal, A. A.; Hess, S. E.; Kogej, T.; Levin, M. D.; Marder, S. R.; McCord-Maughon, D.; Perry, J. W.; Rockel, H.; Rumi, M.; Subramaniam, G.; Webb, W. W.; Wu, X.-L.; Xu, C. *Science* (*Washington, D.C.*) **1998**, *281* (5383), 1653–1656.
(25) Reinhardt, B. A.; Brott, L. L.; Clarson, S. J.; Dillard, A. G.; Bhatt, J. C.; Kannan, R.; Yuan, L.; He, G. S.; Prasad, P. N. *Chem. Mater.* **1998**, *10* (7), 1863–1874.
(26) Rumi, M.; Ehrlich, J. E.; Heikal, A. A.; Perry, J. W.; Barlow, S.; Hu, Z.; McCord-Maughon, D.; Parker, T. C.; Roeckel, H.; Thayumanavan, S.; Marder, S. R.; Beljonne, D.; Bredas, J.-L. *J. Am. Chem. Soc.* **2000**, *122* (39), 9500–9510.
(27) Lu, Y.; Hasegawa, F.; Goto, T.; Ohkuma, S.; Fukuhara, S.; Kawazu, Y.; Totani, K.; Yamashita, T.; Watanabe, T. *J. Lumin.* **2004**, *110* (1−2), 1–10.
(28) Kamada, K.; Ohta, K.; Iwase, Y.; Kondo, K. *Chem. Phys. Lett.* **2003**, *372* (3,4), 386–393.
(29) Xing, J.-F.; Chen, W.-Q.; Gu, J.; Dong, X.-Z.; Takeyasu, N.; Tanaka, T.; Duan, X.-M.; Kawata, S. *J. Mater. Chem.* **2007**, *17* (14), 1433–1438.
(30) Chou, C.-F.; Huang, T.-H.; Lin, J. T.; Hsieh, C.-C.; Lai, C.-H.; Chou, P.-T.; Tsai, C. *Tetrahedron* **2006**, *62* (36), 8467–8473.
(31) Iwase, Y.; Kamada, K.; Ohta, K.; Kondo, K. *J. Mater. Chem.* **2003**, *13* (7), 1575–1581.
(32) Yang, Z.-D.; Feng, J.-K.; Ren, A.-M. *THEOCHEM* **2008**, *848* (1−3), 24–33.
(33) Kontur S., Stelzer, F. Personal communication, unpublished.
(34) Seidl, B.; Liska, R. *Macromol. Chem. Phys.* **2007**, *208* (1), 44–54.
(35) Rosspeintner, A.; Pucher, N.; Griesser, M.; Iskra, K.; Liska, R.; Gescheidt, G. *Macromolecules*, submitted.
(36) Kannan, R.; He, G. S.; Yuan, L.; Xu, F.; Prasad, P. N.; Dombroskie, A. G.; Reinhardt, B. A.; Baur, J. W.; Vaia, R. A.; Tan, L.-S. *Chem. Mater.* **2001**, *13* (5), 1896–1904.
(37) Demas, J. N.; Crosby, G. A. *J. Phys. Chem.* **1971**, *75* (8), 991–1024.
(38) Kotelevskiy, S. I. *J. Lumin.* **1998**, *79*, 211–214.
(39) Ajami, A.; Pucher, N.; Liska, R.; Stampfl, J.; Husinsky, W., manuscript in preparation.
(40) Makarov, N. S.; Drobizhev, M.; Rebane, A. *Opt. Express* **2008**, *16* (6), 4029–4047.
(41) Dolhem, F.; Lievre, C.; Demailly, G. *Tetrahedron* **2002**, *59* (2), 155–164.
(42) Strohriegl, P.; Jesberger, G.; Heinze, J.; Moll, T. *Makromol. Chem.* **1992**, *193* (4), 909–19.
(43) Mitzel, F.; Boudon, C.; Gisselbrecht, J.-P.; Seiler, P.; Gross, M.; Diederich, F. *Helv. Chim. Acta* **2004**, *87* (5), 1130–1157.
(44) Olomucki, M.; Le Gall, J. Y. *Bull. Soc. Chim. Fr.* **1976** (9−10), 1467−8.
(45) Takalo, H.; Kankare, J.; Hanninen, E. *Acta Chem. Scand., Ser. B* **1988**, *B42* (7), 448–54.
(46) Suh, S. C.; Suh, M. C.; Shim, S. C. *Macromol. Chem. Phys.* **1999**, *200* (9), 1991–1997.
(47) Michel, P.; Gennet, D.; Rassat, A. *Tetrahedron Lett.* **1999**, *40* (49), 8575–8578.
(48) Angulo, G.; Grampp, G.; Rosspeintner, A. *Spectrochim. Acta, Part A* **2006**, *65A*, 727–731.
(49) Wang, E. J.; Li, J.; Yang, Y. Y. *J. Photopolym. Sci. Technol.* **1991**, *4* (1), 157–164.
(50) The emission lifetime of O3K was too long ($\tau > 1$ μs) to be measured with the available single photon counting apparatus.
(51) Turro, N. J.; Ramamurthy, V.; Scaiano, J. C. *Principles of Molecular Photochemistry*; University Science Books: Sausalito, CA, 2009; ISBN: 978-1-891389-57-3.
(52) Sheik-bahae, M.; Said, A. A.; Wei, T. H.; Wu, Y. Y.; Hagan, D. J.; Soileau, M. J.; Van Stryland, E. W. *Proc. SPIE—Int. Soc. Opt. Eng.* **1990**, *1148*, 41−51.
(53) Lee, G. J.; Lee, S. H.; Cho, B. R. *Curr. Appl. Phys.* **2004**, *4* (6), 573–576.
(54) Zheng, S.; Beverina, L.; Barlow, S.; Zojer, E.; Fu, J.; Padilha, L. A.; Fink, C.; Kwon, O.; Yi, Y.; Shuai, Z.; Van Stryland, E. W.; Hagan, D. J.; Bredas, J.-L.; Marder, S. R. *Chem. Commun.* (*Cambridge, U.K.*) **2007**, *13*, 1372–1374.
(55) CAD file from: http://www.rhino3d.com/.